JACS
JOURNAL OF THE AMERICAN CHEMICAL SOCIETY

Communication

pubs.acs.org/JACS

Lithographically Defined Macroscale Modulation of Lateral Fluidity and Phase Separation Realized via Patterned Nanoporous Silica-Supported Phospholipid Bilayers

Eric L. Kendall,[†,∥,#] Viviane N. Ngassam,[‡,#] Sean F. Gilmore,[§] C. Jeffrey Brinker,[⊥] and Atul N. Parikh*[,†,‡,§]

[†]Departments of Chemical Engineering and Materials Science, [‡]Biomedical Engineering, and [§]Applied Science, University of California, Davis, California 95616, United States

[∥]Mechanical Engineering Department, University of Maryland, Maryland 20742, United States

[⊥]Departments of Chemical and Nuclear Engineering and Molecular Genetics and Microbiology, University of New Mexico, Albuquerque, New Mexico 87131, United States

Supporting Information

ABSTRACT: Using lithographically defined surfaces consisting of hydrophilic patterns of nanoporous and nonporous (bulk) amorphous silica, we show that fusion of small, unilamellar lipid vesicles produces a single, contiguous, fluid bilayer phase experiencing a predetermined pattern of interfacial interactions. Although long-range lateral fluidity of the bilayer, characterized by fluorescence recovery after photobleaching, indicates a nominally single average diffusion constant, fluorescence microscopy-based measurements of temperature-dependent onset of fluidity reveals a locally enhanced fluidity for bilayer regions supported on nanoporous silica in the vicinity of the fluid−gel transition temperature. Furthermore, thermally quenching lipid bilayers composed of a binary lipid mixture below its apparent miscibility transition temperature induces qualitatively different lateral phase separation in each region of the supported bilayer: The nanoporous substrate produces large, microscopic domains (and domain-aggregates), whereas surface texture characterized by much smaller domains and devoid of any domain-aggregates appears on bulk glass-supported regions of the single-lipid bilayer. Interestingly, lateral distribution of the constituent molecules also reveals an enrichment of gel-phase lipids over nanoporous regions, presumably as a consequence of differential mobilities of constituent lipids across the topographic bulk/nanoporous boundary. Together, these results reveal that subtle local variations in constraints imposed at the bilayer interface, such as by spatial variations in roughness and substrate adhesion, can give rise to significant differences in macroscale biophysical properties of phospholipid bilayers even within a single, contiguous phase.

Tenacious binding of inorganic silica with organic phospholipid assemblies in water enables the class of supported membranes, which has drawn significant practical interest as simplified models of cellular membranes and as components of biosensors and assays of membrane targets.[1] Previous studies indicate that this membrane-substrate adhesion is mediated by a thin layer of water, 0.5−1.5 nm thick, sandwiched between the lipid headgroups and silica.[2] The structure and properties of the sandwiched water layer, however, are not likely to be those of bulk water; rather they are thought to be influenced by the underlying hydroxylated silica surface.[2b] The latter presents a mixture of isolated, geminal, and vicinial silanol (Si−OH) groups (average surface coverage, ∼5 OH/nm^2), surface charge, densities and distributions of which are determined by their unique bimodal (4.5 and 8.5) pK_a behavior.[3]

As a consequence of this water-mediated adhesion of lipid bilayers to silica, supported membranes display significant variability in their biophysical properties in comparison with their "free" counterparts (e.g., suspended lipid bilayers and giant unilamellar vesicles). Specifically, out-of-plane undulations, membrane tension, phase transition, and phase separation characteristics are all modulated in supported systems,[4] which in turn constrain membrane shape transformations and modulate binding properties of membrane receptors.[5] In this vein, colloidal sol−gel silica, synthesized from molecular precursors in the aqueous phase under low temperature and ambient pressure conditions, offers an attractive approach to altering membrane−substrate adhesion characteristics. The sol−gel formation pathway involves a combination of hydrolysis and condensation polymerization reactions,[6] whose kinetics and interplay are readily tunable by manipulation of experimental parameters (e.g., via pH-dependent catalytic control). Thus, silica surfaces exhibiting a broad variety of structure and morphologies can be readily obtained through this route. Furthermore, by recruiting colloidal templates (e.g., micelles) as structure-directing agents, which are preorganized or which co-assemble during silica formation, the range of silica obtained can be elaborated to include exquisitely structured silica consisting of features (e.g., ordered porosity) spanning nanometer to micrometer length scales.[7] Moreover, such sol−gel synthesized silica, owing to the high density of water-filled hydrophilic nanopores at their surface, might afford a better hydrated interface, cushioning the adherent bilayer from the substrate, while providing enhanced structural integrity and stability compared to free bilayers.

Received: August 14, 2013
Published: October 10, 2013

   dx.doi.org/10.1021/ja408434r | J. Am. Chem. Soc. 2013, 135, 15718−15721

Previous studies demonstrate that sol−gel silica offers adhesive preferences for membrane lipids, qualitatively similar to that of bulk silica.[8] Laterally contiguous single-lipid bilayers form readily on planar or spherical sol−gel surfaces by standard vesicle fusion.[8a,b,d] The construct has been shown to afford a robust biomimetic strategy to stably encapsulate cargo and display ligands (e.g., cell targeting, fusogenic, or -PEG-terminated) in a fluid, reconfigurable membrane surface, which can interact multivalently with target cells enabling selective binding and internalization.[8c]

In addition to the presence of ordered porosity, several other surface properties of sol−gel silica are different from the bulk counterpart. These include the density, distributions, and acidity behavior of surface silanols, local surface topographical and "chemical" roughness, and the thickness and structure of the adsorbed/interfacial water layer.[3a,9] How this combination of differences in interfacial properties between solid and nanoporous, sol−gel silica influence membrane physical properties is, however, not yet understood.[4e] Here, we *directly* compare three key biophysical properties, namely lateral fluidity, phase-transition temperature, and lateral phase separation, of single phospholipid bilayers supported on nanoporous silica with those of phospholipid bilayers supported on bulk silica glass in single samples. Using a novel substrate configuration consisting of microscopic spatial patterns of porous and bulk silica surfaces in single samples (see Figure S1 in Supporting Information [SI]), we find that nanoporous silica-supported bilayers exhibit an enhanced lateral fluidity and a significant suppression in the effective gel-fluid transition temperature. Moreover, nanoporous silica-supported mixed composition bilayers exhibit pronounced phase separation characterized by significantly larger, micrometer-scale domains compared to those on bulk glass.

To enable direct comparison between properties of lipid bilayers supported on bulk silica and nanoporous sol−gel silica and to define spatially varied substrate characteristics, we first prepare lateral patterns of thin film silica mesophases (Supporting Methods in SI). This is achieved by simply spin-coating the sol−gel precursor solution (containing surfactant molecules) onto a bulk glass surface modified with an *n*-octadecyl-tricholorosilane (OTS) monolayer that is lithographically exposed to UV−ozone creating spatial patterns of surface wettability. Upon evaporation of ethanol, the precursor solution preferentially wets the exposed, hydrophilic glass regions and recedes and dewets the OTS-covered regions during the spin-coating process. Concurrently, solvent evaporation drives the formation of an ordered silica−surfactant mesophase via evaporation-induced self-assembly.[10] Subsequent uniform exposure to short-wavelength UV radiation (184−257 nm) under oxidative conditions photochemically calcines the surfactant and remaining OTS and promotes further condensation of the siloxane framework to form patterned hydrophilic nanoporous silica patches bounded by bulk silica glass.[10b] A unique feature of this platform is that it enables side-by-side comparison of properties of single-lipid bilayers supported on bulk and nanoporous hydroxylated surfaces obtained through vesicle fusion.

Preliminary characterization of the nanoporous/bulk glass pattern confirms its purported structure. Large area bright-field images reveal the spatial pattern (Figure 1A), and AFM data in Figure 1 (B and D) confirm that the individual nanoporous-supported patches have uniform thickness (~40 nm) with low roughness (r.m.s. roughness, 0.2 ± 0.1 nm) bounded by a tall

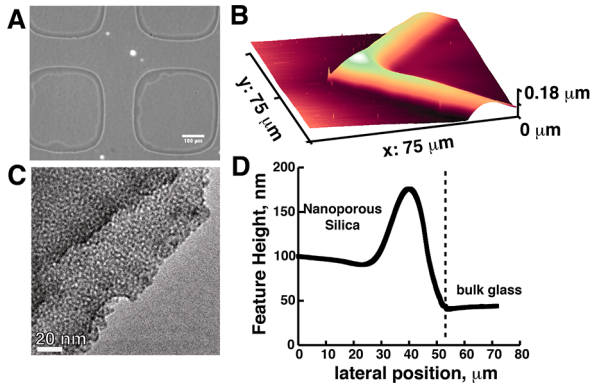

Figure 1. (A) Optical microscopy image showing nanoporous silica patches and the raised rim at the perimeter of each patch, Scale Bar, 100 μm. (B) AFM image showing raised rim. (C) TEM image showing isotropic wormlike nanoporosity of deposited film, Scale Bar, 20 nm. (D) representative AFM trace showing thickness of film.

rim (100−150 nm) at the edges of the nanoporous patch. The presence of tall bounding rims is not surprising since, during spin-coating, the evaporation of volatile components from the edges of a defined patch with fixed contact line should drive interior liquid (together with the sol components) toward the edge by capillary flow; a phenomenon commonly known as the coffee ring effect.[11] TEM microscopy images of scrapings of these thin-film silica mesophases confirm the uniform, isotropic porous nature of the material (Figure 1C) in good agreement with previous reports.[10a] Subsequently, single phospholipid bilayers are prepared by standard vesicle fusion in which the substrate patterns are simply incubated with buffered aqueous dispersions of small unilamellar vesicles (hydrodynamic dia., ~100 nm) composed of the desired lipid mixtures.

Initial experiments employing DMPC (T_m, 24 °C) doped with 1 mol % Texas Red DHPE (TR-DHPE) give rise to a pattern of fluorescence, which replicates the underlying pattern of the substrate type (Figure 2). Uniform fluorescence emission within each of the two distinct regions is consistent with the formation of laterally uniform bilayers spanning both the nanoporous and bulk regions. The enhanced fluorescence intensity (0−10%) from the bilayers on the nanoporous support is likely a result of nonuniform partitioning of TR-DHPE between the two regions and is our first indication that

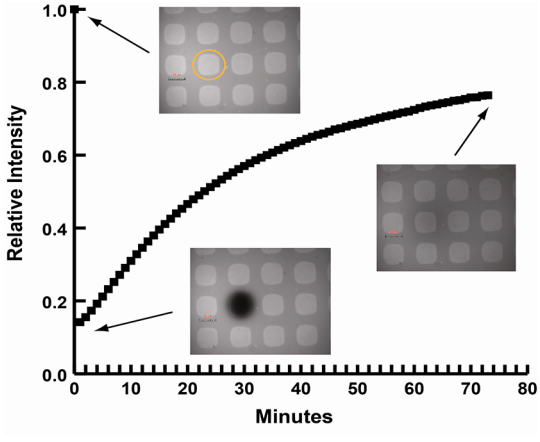

Figure 2. Fluorescence recovery after photobleaching (FRAP) with selected inset micrographs.

dx.doi.org/10.1021/ja408434r | J. Am. Chem. Soc. 2013, 135, 15718−15721

lateral movement of lipids between surface regions is possible. Moreover, because TR-DHPE exhibits a strong preference for the fluid phase of the bilayer, it is also likely that the increased fluorescence intensity from the bilayer on the sol−gel substrate reflects the decreased packing density and therefore increased local fluidity of the bilayer over the topographically roughened porous substrate (see below).

To confirm that the brighter bilayer over the nanoporous support and the dimmer one over bulk glass are contiguous parts of a single-lipid bilayer, we carry out a large-area fluorescence recovery after a photobleaching (FRAP) experiment. A large circular region of the bilayer, encompassing an entire nanoporous silica patch, is photobleached using an intense beam of excitation light for several minutes. Subsequent recovery of the fluorescence intensity in the photobleached region (Figure 2) establishes that the bilayer on the nanoporous silica square is laterally contiguous, exchanging molecules via long-range lateral fluidity, with the surrounding bilayer supported on the bulk glass. Diffusion constants determined using FRAP measurements reveal comparable diffusion constants of D_{mp} = 1.0 ± 0.1 $\mu m^2/s$ and D_{glass} = 1.3 ± 0.2 $\mu m^2/s$ for the DMPC bilayer supported on nanoporous and bulk glass in single samples. Next, to determine if the transition temperature of the bilayer elements supported on the two substrates differed, we carry out a temperature-dependent FRAP experiment.[12] Here, the sample temperature is lowered to 18 °C, below T_m of the DMPC bilayer, and spots are photobleached in the now immobile, gel-phase bilayer in both the nanoporous and bulk glass-supported bilayers

The temperature of the sample is then raised gradually (0.4 °C/min, Figure S4 in SI) and fluorescence intensity in each bleached spot (compared to a reference unbleached spot) is monitored (Figure 3). The temperature-dependent intensity

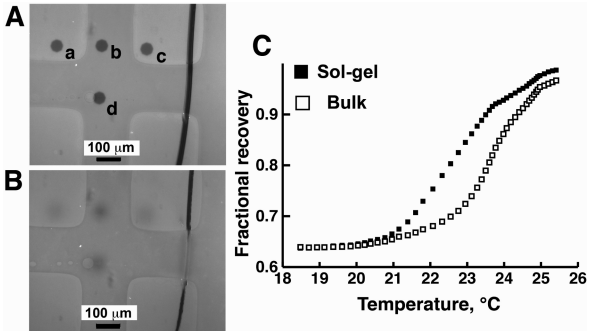

Figure 3. Temperature-dependent fluorescence recovery of bleached spots in a nanoporous and bulk silica-supported gel phase (nonfluid) bilayer. (A) 18.5 °C, (B) 25.3 °C, and (C) fractional recovery profile as a function of temperature.

profile then quantifies the fluidity transition temperature (inflection point) corresponding to the local onset of lateral fluidity. The bilayer supported on nanoporous silica reveals a measurably lower effective transition temperature (~21.9 °C vs 23.8 °C) than the corresponding bulk glass-supported bilayer. This reduction in apparent, local transition temperature agrees well with previous theoretical work in which reduction in adhesion strength, and thus increased fluidity, is predicted for bilayers supported on surfaces characterized by arrays of trenches and pits.[13] Note also that the spatial pattern of fluidity, seemingly determined by the local variations in substrate nanostructure and chemistry, exists within a single contiguous bilayer.

A much more dramatic difference in membrane organization is visible when a bilayer composed of a domain forming mixture such as 2:1 DOPC:DSPC is cooled on the nanoporous/bulk glass pattern (Supporting Videos, 1−3ja408434r_si_002.avi−ja408434r_si_004.avi). Previous studies show that this mixture phase separates when cooled below its miscibility transition temperature in a rate-dependent manner.[8d] Linear cooling (0.2 °C/min) of the mixed bilayer produces large, microscopic domains in the nanoporous supported regions, but no resolvable domains are seen in the bulk glass-supported regions (Figure 4). Lowering the temperature from ~34 to 30 °C in

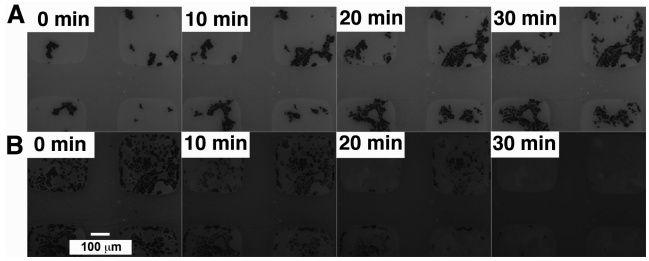

Figure 4. Selected frames from time-lapse fluorescence images acquired during linear thermal trajectory (0.2 °C/min) of 2:1 DOPC:DSPC bilayer on patterned nanoporous/bulk glass substrate: (A) cooling sequence from 33.8 to 29.8 °C and (B) heating sequence from 23 to 55 °C (Supporting Video S1ja408434r_si_002.avi).

real-time (Figures S3 and S4, SI), reveals the appearance, growth, and accumulation of irregularly shaped, dark, microscopic domains (5−1000 μm^2) devoid of fluorescence. Because TR-DHPE partitions preferentially into the fluid phase, the probe-depleted domains can be readily attributed to the gel phase, DSPC lipids at room temperature. AFM images (Figure S2 in SI) yield independent confirmation that the dark, fluorescence-free regions are indeed lipid domains, rather than holes, consistent with findings in a previous study.[8d] Slow nonlinear (Newtonian) cooling at an average rate of 0.1 °C/min of 2:1 DOPC/DSPC lipid bilayers produces qualitatively different results from the fast-cooling experiments (Figure S5 in SI). Here, the domains form in both regions of the sample. For bilayers on nanoporous silica, a bimodal distribution of sizes is evident, consisting of both smaller domains, similar to those found on bulk glass, and large microscopic aggregates. Moreover, area occupancy of domains for nanoporous silica-supported regions of the bilayer is much larger (39%−80%) compared to that over bulk glass (5%−19%).

In subsequent thermal cycles, we find that domains reappear on the sol−gel silica at both the same and new locations and become progressively more numerous occupying a greater proportion of the sol−gel substrate (Figure S6, Supporting Videos S2 and S3 ja408434r_si_003.avi and ja408434r_si_004.avi). Together with the observations that bilayer over the entire composite surface is in a single contiguous phase, this discrepancy in domain population between the bulk and nanoporous glass suggests that the compositional heterogeneity in domain size and density develops between sol−gel and bulk silica. We surmise that this preferential or directed migration of DSPC across the topographical boundary into the nanoporous-supported regions producing a diode-like effect, which results presumably from the patterns of curvatures present at the lithographic boundary.[14]

Results presented here show that subtle differences at the membrane interface with the substrate translate into dramatic differences in lateral fluidities and phase separation in supported membranes. To further consider if these differences originate from differences in chemistry or topography of the underlying substrate, an early report purportedly studying the role of topography in lateral phase separation is particularly instructive. Yoon et al.[15] find that nanometer scale roughness is sufficient to impede the growth of liquid-ordered domains by introducing a bending penalty onto the adhering bilayer producing a seemingly opposite trend viz. large liquid-ordered domains of greater bending rigidity[15b−d] form preferentially on the smooth substrate and domains remain small, because of elastic barrier, on the rough substrate. In our case, physical roughness present because of porosity is much more diminished because of a persistent interfacial water layer resulting from enhanced wettability of the nanoporous hydroxylated sol−gel film. Recall also that the differences in chemistry between the two substrate types are related to the differences in density and acidity of the silanol groups as well as the thickness and structure of the adsorbed water layer. These differences thus translate into differences in membrane−substrate adhesion energy. On the basis of the above factors, we reason that it is the ability of the bilayer to bridge across the pores of the sol−gel substrate supported on an interfacial water layer, and the resultant reduction in lipid−silica interaction, that gives rise to reduced adhesion, which, in agreement with theory, drives the observed enhancement in lateral fluidity and preferential partitioning of gel phase lipids into nanoporous regions.

A corollary finding, which emerges from this study, is that the effect of interfacial interactions is highly local, producing spatial regions of coexisting physical properties within the single-lipid bilayer phase. The correspondence of this interfacial nanostructure-dependent amplification of lateral fluidity and phase separation propensity with natural cytoskeleton-supported lipid bilayers is unknown, but we suspect that nature has discovered this behavior before us.

■ ASSOCIATED CONTENT

Ⓢ Supporting Information

Supplementary methods, supporting atomic force microscopy data, and three time-lapse fluorescence movies (ja408434r_si_002.avi−ja408434r_si_004.avi). This material is available free of charge via the Internet at http://pubs.acs.org.

■ AUTHOR INFORMATION

Corresponding Author

anparikh@ucdavis.edu

Author Contributions

#E.L.K. and V.N.N. contributed equally.

Notes

The authors declare no competing financial interest.

■ ACKNOWLEDGMENTS

We thank J. Roehling for help with TEM measurements. This work is supported by the U.S. Department of Energy, BES, Division of Materials Science & Engineering under Award DE-FG02-04ER46173. C.J.B. acknowledges support from U.S. DOE, Office of Science, Office of Basic Energy Sciences, Division of Materials Sciences and Engineering, NCI Cancer Nanotechnology Platform Partnership grant 1U01CA151792-01, Sandia LDRD, AFOSR grant FA 9550-10-1-0054, and NSF/EPA DBI 0830117.

■ REFERENCES

(1) (a) Sackmann, E. *Science* **1996**, *271*, 43−48. (b) Castellana, E. T.; Cremer, P. S. *Surf. Sci. Rep.* **2006**, *61*, 429−444.

(2) (a) Bayerl, T. M.; Bloom, M. *Biophys. J.*. **1990**, *58*, 357−362. (b) Kim, J.; Kim, G.; Cremer, P. S. *Langmuir* **2001**, *17*, 7255−7260.

(3) (a) Zhuravlev, L. T. *Colloid Surf. A* **2000**, *173*, 1−38. (b) Leung, K.; Nielsen, I. M. B.; Criscenti, L. J. *J. Am. Chem. Soc.* **2009**, *131*, 18358−18365.

(4) (a) Czolkos, I.; Jesorka, A.; Orwar, O. *Soft Matter* **2011**, *7*, 4562−4576. (b) Stottrup, B. L.; Veatch, S. L.; Keller, S. L. *Biophys. J.*. **2004**, *86*, 2942−2950. (c) Liu, J.; Conboy, J. C. *J. Am. Chem. Soc.* **2004**, *126*, 8894−8895. (d) Xie, A. F.; Yamada, R.; Gewirth, A. A.; Granick, S. *Phys. Rev. Lett.* **2002**, 89. (e) Varma, S.; Teng, M.; Scottt, H. L. *Langmuir* **2012**, *28*, 2842−2848.

(5) (a) Lipowsky, R. *Faraday Discuss.* **2013**, *161*, 305−331. (b) Jung, H.; Robison, A. D.; Cremer, P. S. *J. Struct. Biol.* **2009**, *168*, 90−94.

(6) (a) Brinker, C. J. *J. Non-Cryst. Sol.* **1988**, *100*, 31−50. (b) Livage, J.; Sanchez, C. *J. Non-Cryst. Sol.* **1992**, *145*, 11−19.

(7) (a) Mann, S.; Burkett, S. L.; Davis, S. A.; Fowler, C. E.; Mendelson, N. H.; Sims, S. D.; Walsh, D.; Whilton, N. T. *Chem. Mater.* **1997**, *9*, 2300−2310. (b) Raman, N. K.; Anderson, M. T.; Brinker, C. J. *Chem. Mater.* **1996**, *8*, 1682−1701.

(8) (a) Doshi, D. A.; Dattelbaum, A. M.; Watkins, E. B.; Brinker, C. J.; Swanson, B. I.; Shreve, A. P.; Parikh, A. N.; Majewski, J. *Langmuir* **2005**, *21*, 2865−2870. (b) Nellis, B. A.; Satcher, J. H.; Risbud, S. H. *ACTA Biomater.* **2011**, *7*, 380−386. (c) Ashley, C. E.; Carnes, E. C.; Phillips, G. K.; Padilla, D.; Durfee, P. N.; Brown, P. A.; Hanna, T. N.; Liu, J. W.; Phillips, B.; Carter, M. B.; Carroll, N. J.; Jiang, X. M.; Dunphy, D. R.; Willman, C. L.; Petsev, D. N.; Evans, D. G.; Parikh, A. N.; Chackerian, B.; Wharton, W.; Peabody, D. S.; Brinker, C. J. *Nat. Mater.* **2011**, *10*, 389−397. (d) Goksu, E. I.; Nellis, B. A.; Lin, W. C.; Satcher, J. H.; Groves, J. T.; Risbud, S. H.; Longo, M. L. *Langmuir* **2009**, *25*, 3713−3717.

(9) Gallas, J. P.; Goupil, J. M.; Vimont, A.; Lavalley, J. C.; Gil, B.; Gilson, J. P.; Miserque, O. *Langmuir* **2009**, *25*, 5825−5834.

(10) (a) Lu, Y. F.; Ganguli, R.; Drewien, C. A.; Anderson, M. T.; Brinker, C. J.; Gong, W. L.; Guo, Y. X.; Soyez, H.; Dunn, B.; Huang, M. H.; Zink, J. I. *Nature* **1997**, *389*, 364−368. (b) Clark, T.; Ruiz, J. D.; Fan, H. Y.; Brinker, C. J.; Swanson, B. I.; Parikh, A. N. *Chem. Mater.* **2000**, *12*, 3879−3884.

(11) Deegan, R. D.; Bakajin, O.; Dupont, T. F.; Huber, G.; Nagel, S. R.; Witten, T. A. *Nature* **1997**, *389*, 827−829.

(12) Smith, A. M.; Vinchurkar, M.; Gronbech-Jensen, N.; Parikh, A. N. *J. Am. Chem. Soc.* **2010**, *132*, 9320−9327.

(13) Swain, P. S.; Andelman, D. *Langmuir* **1999**, *15*, 8902−8914.

(14) (a) Hsieh, W. T.; Hsu, C. J.; Capraro, B. R.; Wu, T. T.; Chen, C. M.; Yang, S.; Baumgart, T. *Langmuir* **2012**, *28*, 12838−12843. (b) Roder, F.; Birkholz, O.; Beutel, O.; Paterok, D.; Piehler, J. *J. Am. Chem. Soc.* **2013**, *135*, 1189−1192. (c) Ogunyankin, M. O.; Longo, M. L. *Analyst* **2013**, *138*, 3719−3727.

(15) (a) Yoon, T. Y.; Jeong, C.; Lee, S. W.; Kim, J. H.; Choi, M. C.; Kim, S. J.; Kim, M. W.; Lee, S. D. *Nat. Mater.* **2006**, *5*, 281−285. (b) Ogunyankin, M. O.; Torres, A.; Yaghmaie, F.; Longo, M. L. *Langmuir* **2012**, *28*, 7107−7113.